On the Aerodynamics of Tractor-Trailers

M. Hammache and F. Browand

Dept. of Aerospace and Mechanical Engineering, University of Southern California

Abstract

Wind tunnel experiments on the aerodynamics of tractor-trailer models show that the drag on the model is sensitive to the width of the tractor-trailer gap (G) and to the angle of yaw with respect to wind direction. At zero-yaw, relatively low drag is measured up to a critical gap width $G/\sqrt{A} \approx 0.5$, where A is the cross-sectional area. At the critical width the drag experiences a sharp and large increase; most of the drag contribution is attributed to the trailer alone. As the gap is widened further, tractor and trailer become increasingly decoupled from each other and the drag reaches a near-plateau, rising much more gradually.

DPIV measurements in horizontal planes in the gap show that the flow is steady and consists of a relatively stable, symmetric toroidal vortex when the width is below critical. The symmetry breaks down at the critical gap, as evidenced by intermittent ejections of flow from the cavity to either side of the model. These ejections are believed to be at the origin of the sharp increase in trailer drag. As the gap width is increased further, the nature of the flow transitions from cavity-like to wake-like.

These observations can be qualitatively extended to moderate yaw angles (up to ~4 degrees), but the size of the critical gap width diminishes with yaw angle. At higher angles, the drag rises much faster with gap width.

The second part of this paper discusses the drag savings that can be realized by arranging two truck-like models in a tandem. Four tandems were formed by combining two models; each of the models was either "rounded" (i.e. lower drag) or "blunt" (higher drag). The drag of any tandem is generally lower than the sum of the drags of the models in isolation. However, the drag savings also depends on the choice of models (rounded vs. blunt) and on which model is placed in front. A rounded model followed by a blunt model achieves the most relative drag savings, while reversing the order produces the tandem with the least savings.

R. McCallen et al. (eds.), *The Aerodynamics of Heavy Vehicles: Trucks, Buses, and Trains*
© Springer-Verlag Berlin Heidelberg 2004

Introduction

At typical cruising highway speeds, most of the fuel consumed by a large scale road vehicle is expended to simply overcome aerodynamic drag, even in the absence of unfavorable wind conditions. The remaining fuel expenditure is needed to overcome the rolling resistance on tires and internal losses. The fuel efficiency of tractor-trailers, which account for the greatest portion of heavy vehicle traffic by a large margin, is influenced by the shape and physical dimensions of these vehicles. Shape and scale are themselves severely constrained by economic considerations (the parallelepiped shape of trailers is meant to optimize volume loading) and by regulatory constraints (truck dimensions are fixed and drag-reduction devices cannot exceed specified limits).

A look at the evolution of tractor-trailer design over the last several decades reveals gradual aerodynamic improvements to the front of vehicles, namely from the front of the tractor to the front of the trailer, but very little has been done to improve the back of trailers. Tractors have benefited from tremendous improvements, such as the adoption of the aero-shield as an integrated part of the cab. The problem of the gap between tractor and trailer, which is an important source of drag, has been partly mitigated by the introduction of cab extenders that effectively reduce the size of the gap but do not eliminate it entirely.

In contrast, trailers have seen little modification, aside from the rounding of their vertical leading edges in the front. The fact that hard-shell trailers are designed to be loaded from the back makes the implementation of drag reduction devices in the back particularly challenging. Truck operators are extremely reluctant to deal with any type of physical device that may interfere with routine loading and unloading operations.

The main objective of this paper is to investigate the impact of tractor-trailer gap width on the drag forces experienced by a truck. The study relies on detailed measurements performed on truck models in a wind tunnel. These models are not replicas of actual trucks that can be seen on the roads, but rather truck-like shapes. While these shapes are simplified to the extent that they do not incorporate any of the secondary features of real vehicles (such as mirrors, handlebars, cab extenders, etc...), they do capture the first order effects that account for virtually all aerodynamic forces acting on a real truck. Also, it is worth noting that Reynolds number matching is not achievable in our flow facility because of limitations on model size and flow speeds. However, the experiments discussed here are not meant to simulate the flow around an actual tractor trailer. Instead, the goal is to unveil relevant flow physics that can be generalized, at least to a first order, to higher Reynolds numbers. The simplified shapes also have the advantage of lending themselves to numerical computations. The elimination of detailed features on the models allows numerical computations to be conducted without the costly burden of

complicated grids. As a result, the present data constitutes a suitable benchmark for various Computational Fluid Dynamics codes.

The truck models were mounted on a turn-table, which allows simulations of side wind by turning the truck with respect to the incoming free-stream. The turntable rotation is motorized and allows wind tunnel tests to be performed at angles of yaw up to 30 degrees. Digital particle image velocimetry (DPIV) measurements were obtained of the flow field in the gap between tractor and trailer at different combinations of gap width and angle of yaw. The tractor and trailer were mounted on separate force balances that measured three forces (drag, side and lift) and three moments (yawing, pitching and rolling), although this paper is restricted to a discussion of drag and side force measurements. The use of two separate balances allowed a better understanding of the respective contributions of tractor and trailer aerodynamic loads to the aggregate loads exerted on the truck as a whole.

In the second part of this paper, we examine the aerodynamic drag of two trucks in a tandem configuration at zero-yaw. Considerable fuel savings for each vehicle in a platoon of road vehicles (in comparison to the same vehicles traveling in isolation) have been observed in the past. The present experiments serve to quantify the drag savings and unveil some surprising and counter-intuitive characteristics of dual-vehicle platoons. Some of these results are believed to be applicable to multi-vehicle platoons as well.

The flow facility

Experiments were conducted in the test section of the Dryden wind tunnel at USC, a re-circulating flow facility with a top speed of 30 m/s. The test section is octagonal in cross section; the sides of the octagon are 1.37 m apart. For the purpose of ground vehicle studies, a ground-plane has been placed in the wind tunnel such that 5 sides of the octagon lie above the plane. The ground-plane is actually a shallow box that spans the width of the wind tunnel, 1.37 m, and is approximately 5.8 m in length. The ground-plane box houses a stepper-motor-controlled traverse that opens and closes the gap by moving the trailer in the downstream direction. The position of the tractor is fixed. Both tractor and trailer rest on an interior turntable of diameter 1.22 m to allow the models to be yawed with respect to the flow direction, as shown in Figure 1. The ground-plane box is mounted in the tunnel at a very slight angle of attack (one degree) to compensate for boundary layer growth on the walls of the wind tunnel. The front edge of the box, which is aligned with the end of the contraction section and the beginning of the test section, is rounded to avoid leading-edge separation. The surface of the ground-plane consists of a sandwich of punched plates—the smallest holes, 1mm in diameter on 4 mm centers, are in the topmost plate. Slight suction is applied to the plenum below the porous top surface to maintain a thin boundary layer. The pressure gradient, dC_p/dx—measured along the wind tunnel ceiling—is approximately zero (±0.003/m) when the tunnel is empty.

The measurements are performed at a wind tunnel speed of approximately 26 m/s. The model Reynolds number for the tests, based upon the square root of the truck cross-sectional area, √A, is about 310,000.

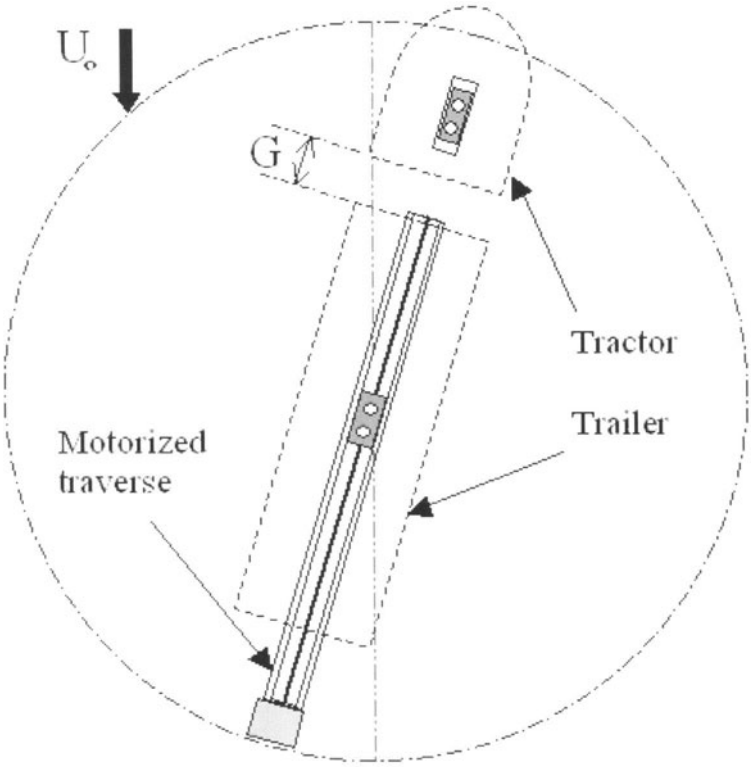

Figure 1. Detail of turntable and traverse mechanism inside ground plane.

The truck models

All models are made of high-density Spyder-foam and machined on a CNC machine. The use of this material allows for rapid prototyping, whereby the shape could be modified quickly and accurately, which reduces turnaround time. The models are roughly 1/15-scale, with no linkage between tractor and trailer. Figure 2 shows a schematic of the tractor and trailer shapes. The tractor model is covered with netting material that consists of a thin plastic mesh. Thanks to the netting, the tractor surface is made rough, which keeps the boundary layer attached but makes the boundary layer thicker. The vertical leading edges of the tractor are rounded to a radius of curvature of 4.55 cm to keep the flow from separating prematurely.

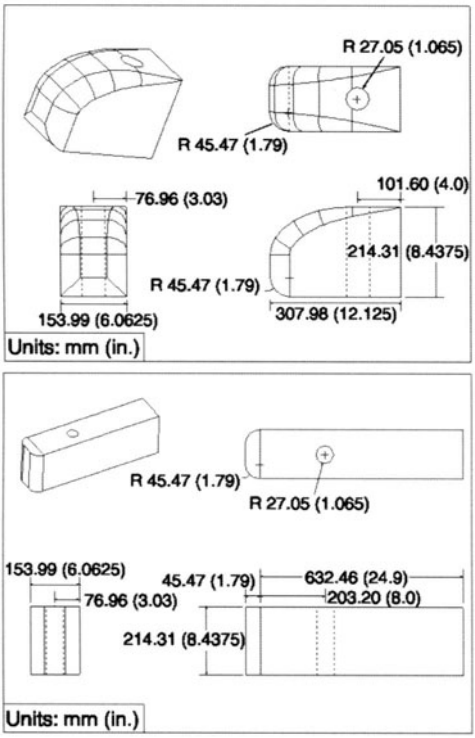

Figure 2. Schematics of tractor and trailer with dimensions.

As Figure 1 illustrates, the position of the tractor is fixed with respect to the turn-table, while the trailer is mounted on a motorized traverse so that the gap width between the two bodies can be varied continuously. The vertical leading edges on the front face of the trailer are also rounded with a radius of curvature of 4.55 cm.

The effect of leading edge rounding on the drag

The drag of a road vehicle (or any body shape in general) is greatly influenced by the degree of bluntness at the front end, e.g. Cooper (1985). In the present case, the degree of bluntness is determined by the radius of curvature at the leading-edges of the tractor and trailer. The optimal radius of curvature was estimated by conducting experiments on a number of tractors having varying radii of curvature. The drag was measured for these shapes as a function of wind tunnel speed. Given wind velocity, U, two Reynolds numbers can be defined; one based on the square-root of the cross-sectional area ($Re_A = U\sqrt{A}/\nu$), and the other based on the radius of curvature of the front leading edges ($Re_R = UR/\nu$).

The importance of leading-edge rounding is demonstrated in Figure 3, which is a plot of drag coefficient of an isolated tractor for two values of the radius of curvature over a range of velocities. The tractor with a less blunt

front end (larger radius of curvature) experiences considerably less drag. Here, the data is plotted versus Re_A. Plotting the same data against Re_R, as shown in Figure 4, essentially collapses the two curves on each other. Hence, the radius of curvature appears to be a more appropriate length scale for this flow. Also, note that the drag bottoms out at approximately Re_R = 70,000. This suggests that the flow is not prone to leading edge separation above this critical Reynolds number, and that further rounding of the front end would not lower the drag.

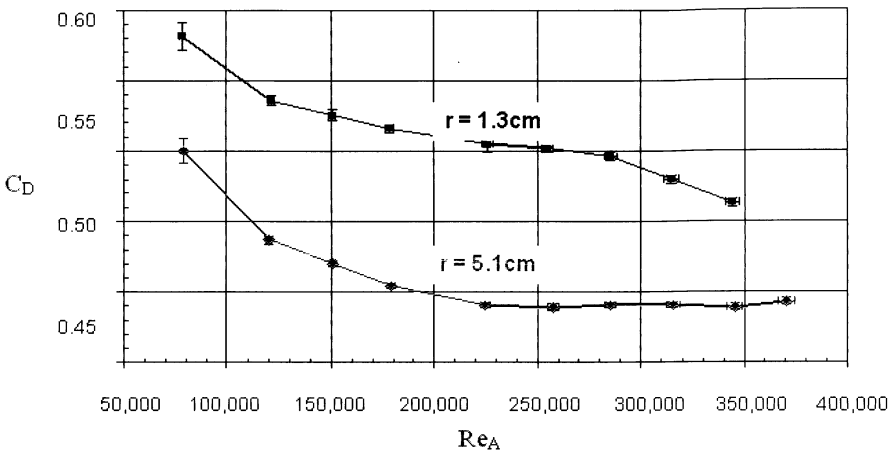

Figure 3. Drag coefficient on isolated tractor as a function of Reynolds number based on square-root of cross-section area for two values of front radius of curvature. Red: r=5.1cm; Blue: r=1.3cm.

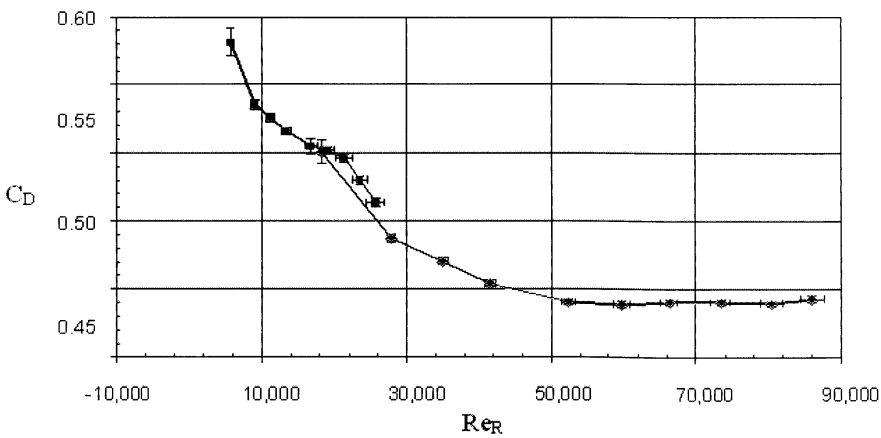

Figure 4. Drag coefficient on isolated tractor as a function of Reynolds number based on front radius of curvature. Red: r=5.1cm; Blue: r=1.3cm.

Drag coefficient versus gap width

The drag on the tractor and trailer as a function of gap width are plotted in Figure 5. In the range of G/√A of 0.1 to 0.5, the trailer experiences less drag than the tractor, due to the shielding effect. Note that at very small gap width, below 0.1, the reverse is true. The extreme proximity of the tractor essentially raises the base pressure on the tractor and reduces its drag. A similar phenomenon can be expected in car racing; the trailing car can take advantage of the suction effect obtained in drafting, but if the gap is reduced below a critical value, the lower drag advantage shifts to the lead car.

As the gap opens up beyond approximately 0.5, the drag on the trailer experiences a dramatic increase. This increase persists up to G/√A of approximately 0.7, then stabilizes (or at least slows down its ascent). At the same time, the tractor also sees a very modest increase then decrease in drag. As the gap width is increased, the trailer contribution to total drag is by far the major one.

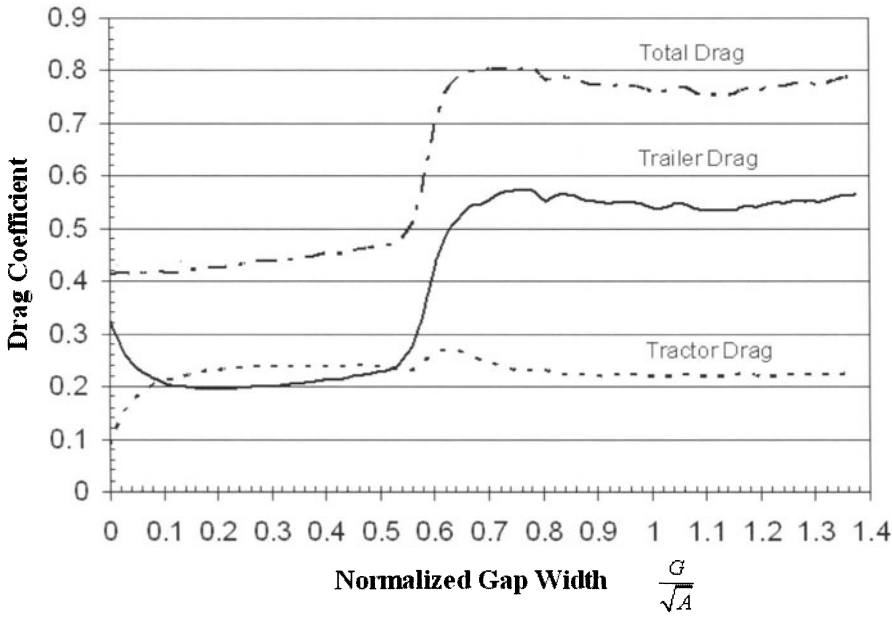

Figure 5. Drag coefficient versus gap width.

DPIV measurements in the gap of a single tractor-trailer

Whole-field velocity measurements were obtained for various combinations of gap width and angles of yaw, though the present discussion is limited to zero-yaw cases. A total of 350 instantaneous realizations were acquired for each case. A detailed discussion of the DPIV technique can be found in Fincham & Spedding (1997). Changes of the flow structure in the gap region were

investigated by performing conditional-averaging. At low gap width, typically below $G/\sqrt{A} \sim 0.5$, the flow is generally steady and consists of what looks like a toroidal vortex in the gap. A horizontal slice through the gap at mid-height shows a symmetric flow field. The average velocity field and associated streamline patterns are shown in Figure 6. The pair of counter-rotating vortices seen in this figure is relatively steady in the sense that all instantaneous realizations are very similar to the average flow field.

As the gap width is increased, the flow in the gap is symmetric part of the time only. Intermittent symmetry breakdown is observed, whereby the flow exits the gap region as shown in Figures 7 through 9. Hence a conditional average of these datasets is labeled "asymmetric flow". Note that the onset of this asymmetry coincides with the initial rise in drag on the trailer and persists until the normalized gap width reaches approximately 1.0, where the flow is once again mostly symmetric. This is shown in Figure 10. Drag measurements such as those in Figure 5 indicate that the drag has reached a high plateau and that restoration of a symmetric flow pattern (on average) is not accompanied by a decrease in drag. At higher gap width, the flow structure is best described by a "wake mode" than "cavity mode" because the gap is so large that the flow pattern is no longer influenced by the proximity of the trailer to the tractor.

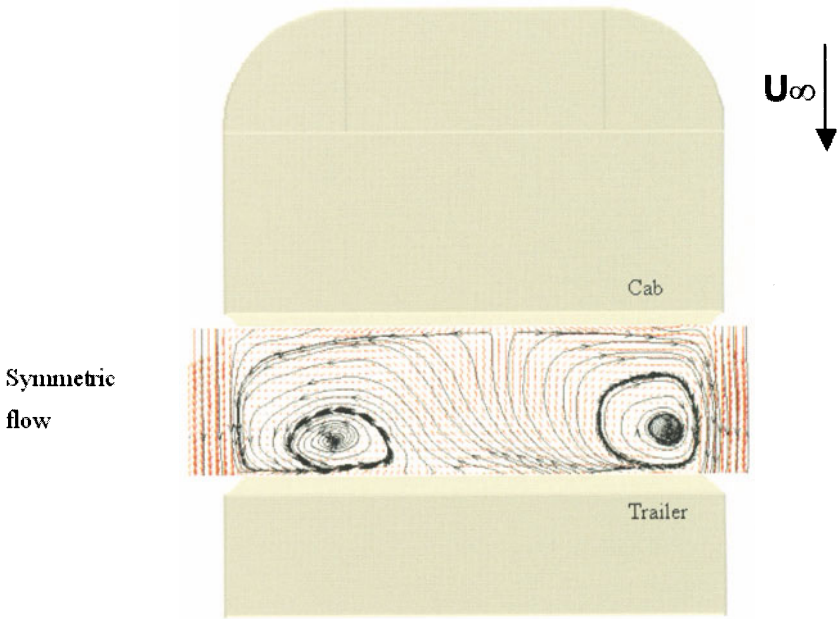

Figure 6. Time-averaged streamline patterns of the flow in the gap at zero yaw, $G/\sqrt{A} = 0.28$.

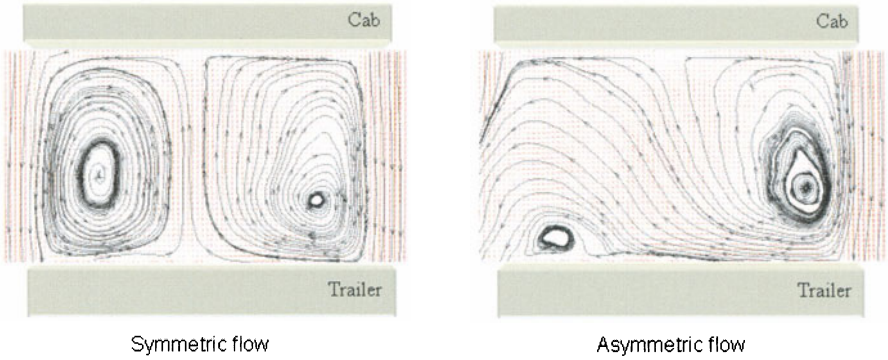

Figure 7. Ensemble-averaged streamline patterns of the flow in the gap at zero yaw, $G/\sqrt{A} = 0.55$. (a) symmetric flow, (b) asymmetric flow.

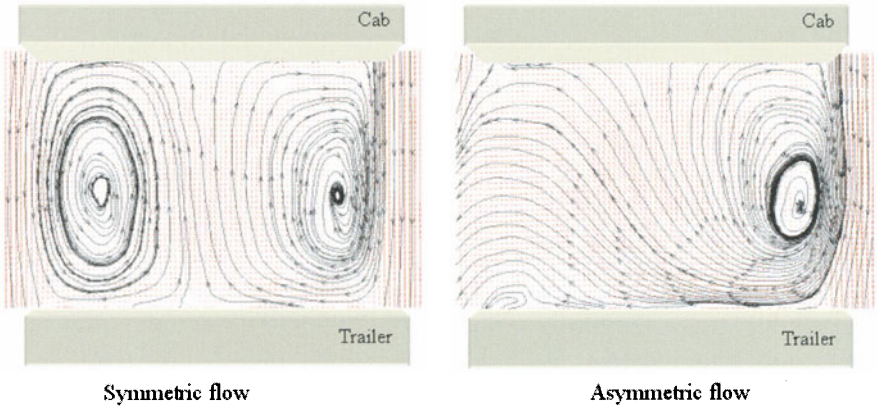

Figure 8. Ensemble-averaged streamline patterns of the flow in the gap at zero yaw, $G/\sqrt{A} = 0.65$. (a) symmetric flow, (b) asymmetric flow.

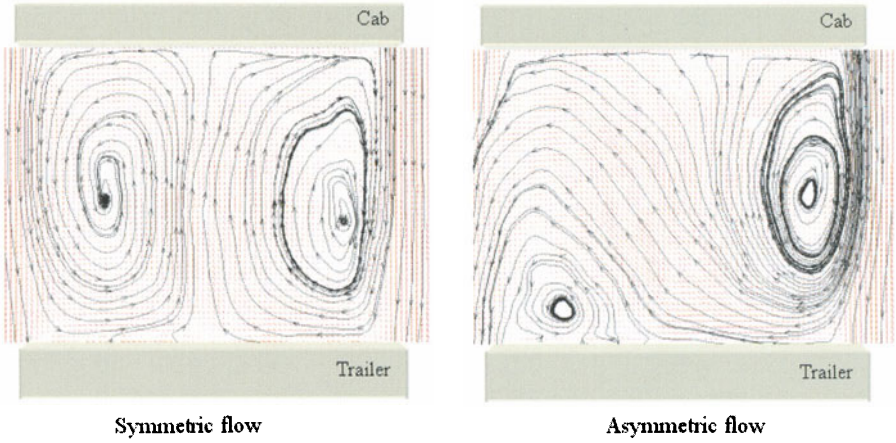

Figure 9. Ensemble-averaged streamline patterns of the flow in the gap at zero yaw, $G/\sqrt{A} = 0.75$. (a) symmetric flow, (b) asymmetric flow.

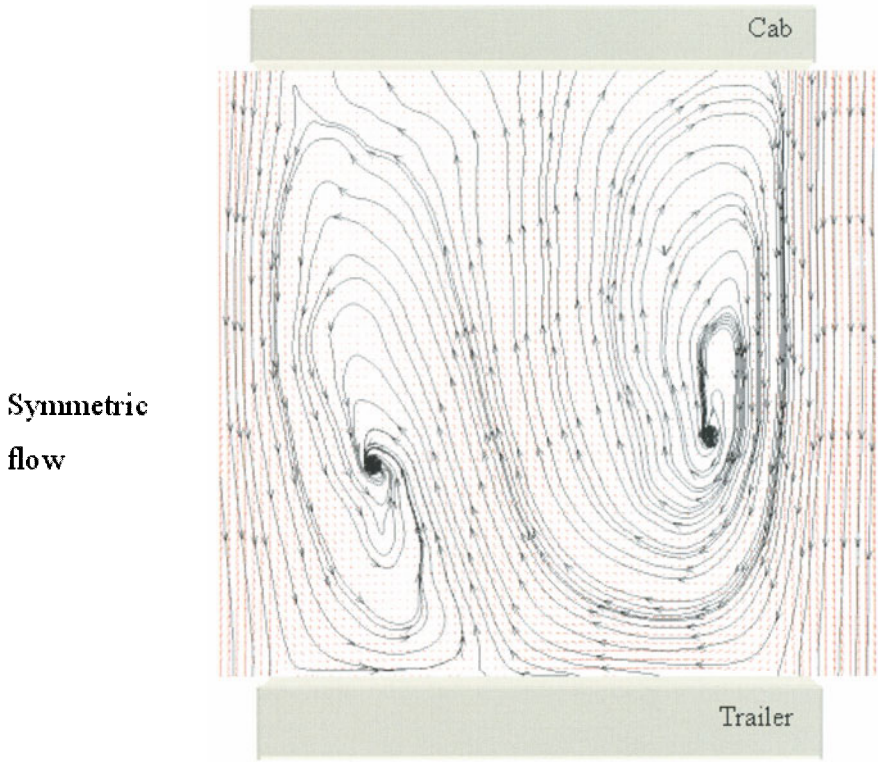

Figure 10. Ensemble-averaged streamline patterns of the flow in the gap at zero yaw, $G/\sqrt{A} = 1.0$.

Hence, over a relatively narrow range of gap width, the truck experiences a dramatic increase in drag. In addition, both drag and side forces are characterized by a substantial increase in fluctuation levels, such that the entire truck undergoes intermittent shaking. This is illustrated by Figure 11, which represents time series of drag force on the trailer at sub-critical and critical gap width. As the gap increases, note that the drag starts out relatively steady then exhibits large-scale, low-frequency oscillations when the critical gap width is achieved. Furthermore, the oscillation amplitude varies with time. Over the first five seconds of data in the bottom plot of Figure 11, the gap flow is symmetric and oscillation amplitude is low, while the next five seconds show higher amplitude as the flow goes asymmetric.

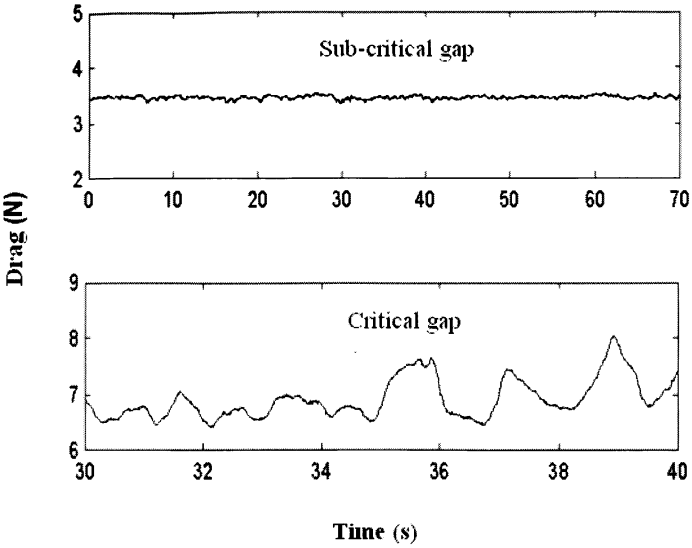

Figure 11. Time series of drag on trailer at sub-critical (top) and critical (bottom) gap width. Bottom plot is a portion of a longer time series.

Drag and side force measurements

The drag data shown in Figure 5 is limited to zero-yaw cases. Similar measurements were performed for both drag and side force over a range of gap width and angles of yaw. The drag data is shown in Figure 12 and that of side forces in Figure 13. The angle of yaw is varied in the range zero to 16 degrees, in increments of one and two degrees. At each yawed position, the non-dimensional gap width $G/\sqrt{A}$ is increased from zero to a maximum value of 1.6 then reduced back to zero. As a result, all the surface maps are roughly symmetric with respect to a vertical plane as illustrated in Figure 12(a). However, due to hysteresis effects, small differences in drag and side force levels are observed in some cases as the gap is opened or closed.

The drag on the tractor increases with the angle of yaw. In addition, it exhibits a peak as shown by a ridge along a line of approximately constant $G/\sqrt{A}$. As was shown in Figure 5 in the zero-yaw case, this maximum is reached when the gap width is approximately half the square-root of frontal area. At higher angles of yaw, the location of the peak shifts to smaller gap widths. Note that at higher yaw angles, the drag drops from its peak, but eventually resumes its ascent. This is seen along the line $G/\sqrt{A}=1.6$. It is likely that the tractor drag will increase further than shown here if $G/\sqrt{A}$ is increased further.

The trailer drag data is plotted in Figure 12(b). Again, the presence of a localized 'ridge' along which the drag reaches a local maximum can be seen, in particular for yaw angles above approx. 6 degrees. However, beyond this ridge, the drag on the trailer does not drop from its peak. It either stays at a plateau

level (angles below approx. 6 degrees) or increases further (angles above approx. 6 degrees).

As Figure 12(c) shows, the drag of the entire truck (which is the sum of the tractor and trailer drag contributions) is accounted for mostly by the drag of the trailer to a greater extent as the gap width and/or yaw angle are increased, which suggests that the drag increases as the two parts are increasingly decoupled and lose the mutual benefit of close formation.

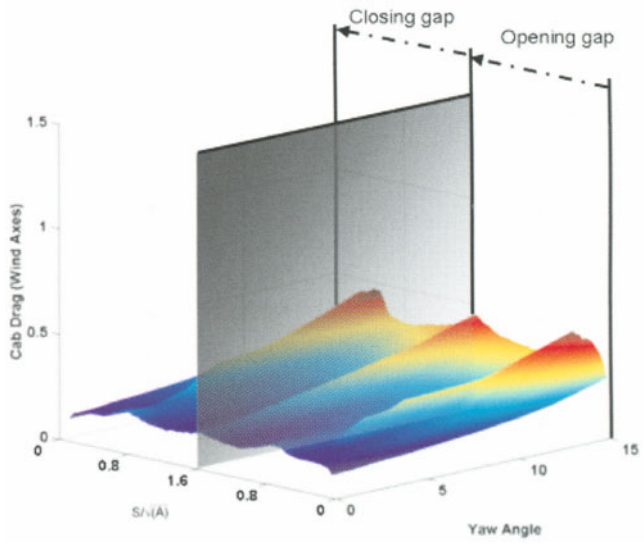

(a)

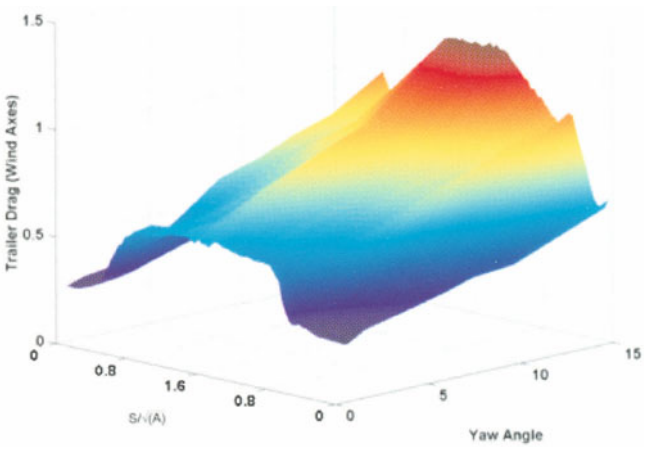

(b)

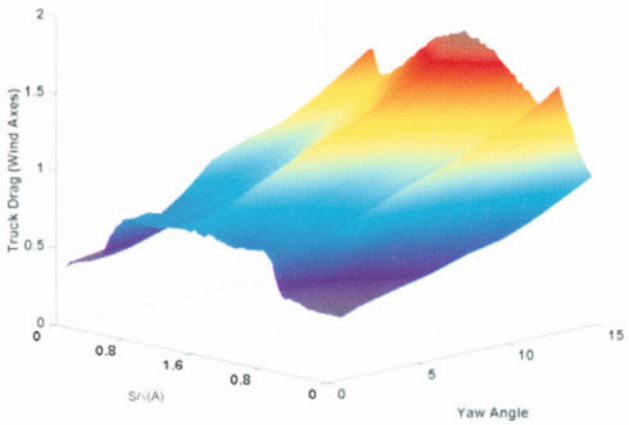

(c)

Figure 12. Surface maps of drag force on tractor (a), trailer (b) and entire truck (c) as a function of yaw angle and gap width.

Figure 13 is a plot of the side force using the same conventions as in Figure 12. The same nearly-constant G/√A "ridge" identified earlier is again seen here. However, the cab experiences a decrease in side force along this ridge, while the trailer experiences an increase. The side force on the whole truck (obtained by adding the two side forces on tractor and trailer) almost eliminates the ridge (with the exception of angles of yaw at the upper end of the range). The total side force is independent of gap width and increases with angle of yaw.

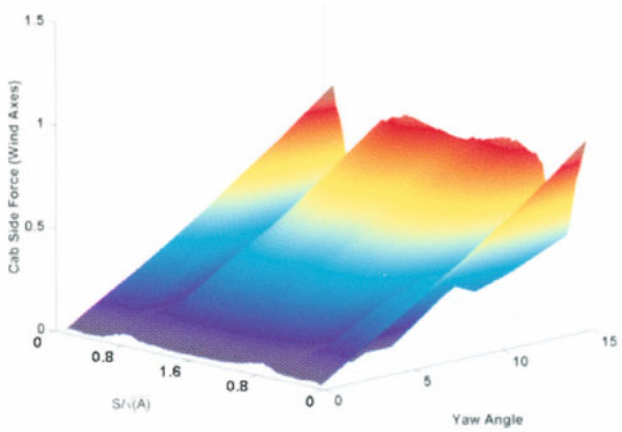

(a)

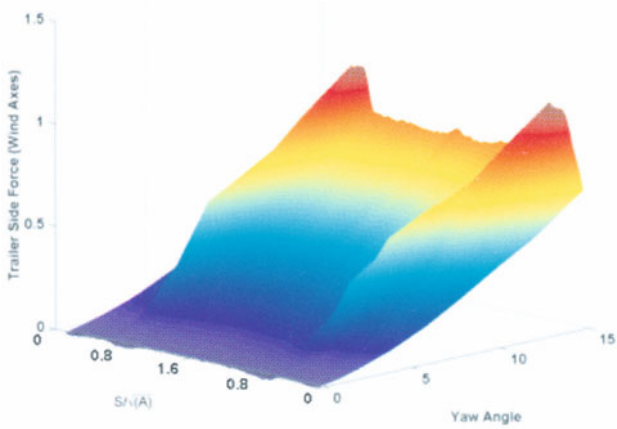

(b)

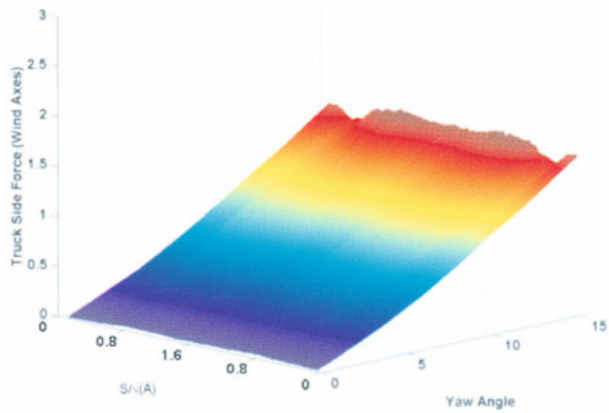

(c)

Figure 13. Surface maps of side force on tractor (a), trailer (b) and entire truck (c) as a function of yaw angle and gap width.

Two trucks in tandem

As stated above, the drag of a truck is largely influenced by the gap width between tractor and trailer. A natural extension of the present study is to examine the drag acting on two trucks in a tandem configuration as a function of the gap separating them. Since all models have the same cross-sectional area (A), gap separation is again divided by √A to make it non-dimensional. All measurements are restricted to zero angles of yaw.

Since trucks are designed to carry cargo, it is important to preserve the box-like shape that characterizes the trailer. Hence, it is worthwhile to study

the drag behavior of *simplified shapes* before conducting experiments on the actual truck models. The simplest shape that can be studied is a simple parallelepiped, which would also be the least aerodynamic. This shape is shown in Figure 14(a) with contributions from fore-body drag, base drag and skin friction. The simplest modification involves adding a faceplate with rounded vertical edges, such that the critical edge Reynolds number mentioned earlier is achieved. This shape is shown in Figure 15(b). Adding the faceplate dramatically reduces drag without compromising the volume-maximizing shape of the body.

Clearly, the drag acting on these bodies is mostly pressure drag; skin friction is minimal. Adding the faceplate reduces the drag by about half, due to a substantial drop in the fore-body pressure drag. This further illustrates the importance of front-end rounding discussed earlier.

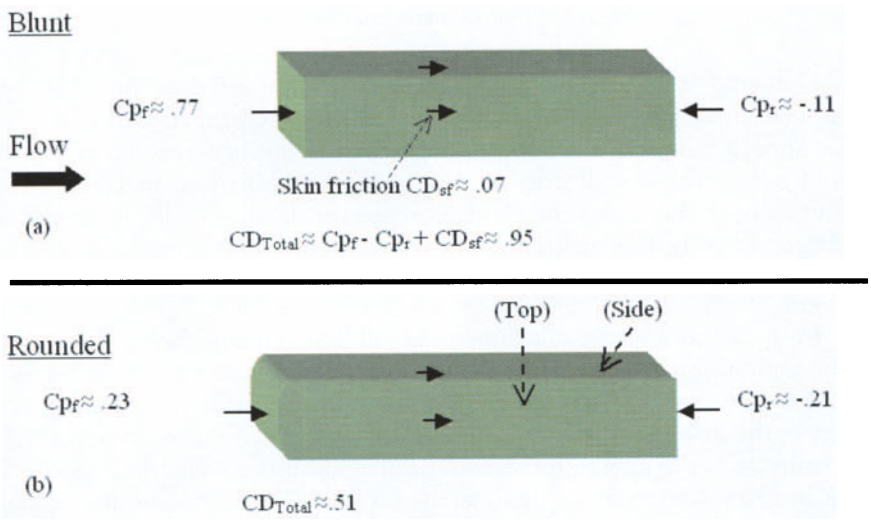

Figure 14. Two basic shapes: (a) a simple parallelepiped; (b) same parallelepiped but with rounded vertical front edges.

The two simple body geometries can be arranged in four possible combinations, depending on which body is put in the lead position, as shown in Figure 15, and the drag acting on each body is measured separately as a function of the gap separating the two bodies. An average drag for the pair of bodies is defined as the sum of the individual drags in the tandem divided by the sum of the individual drags in isolation.

$$CD_{Avg} = (CD_F + CD_R)/(CD_{F\ iso} + CD_{R\ iso})$$

The drag in isolation is defined as the drag of a body alone in the wind tunnel.

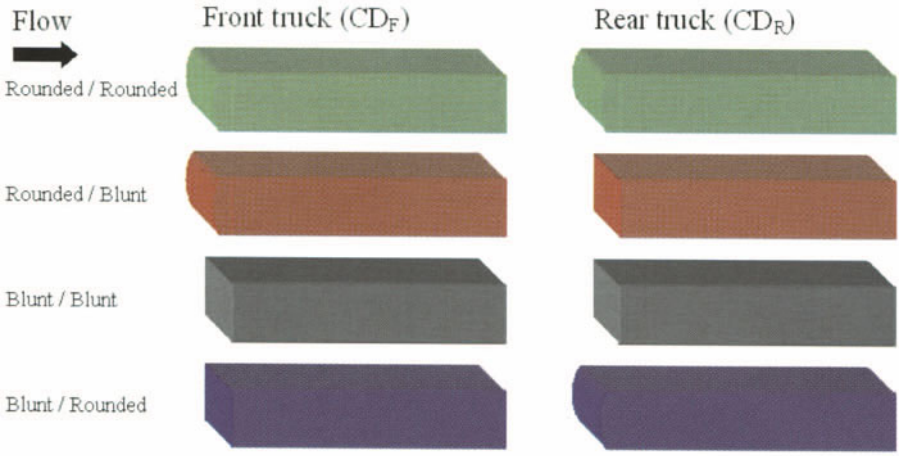

Figure 15. Various tandem combinations.

The goal is to determine the lowest amount of drag possible for a combination of such bodies. It is expected that the proper choice of which body should lead and of the optimal gap separation between the two bodies would reduce the overall drag of the tandem combination. In Figures 16(a) through 16(d), the circles and triangles represent the drag of the front and rear body respectively (normalized by the corresponding drag in isolation) as a function of separation, whereas the solid line represents the average drag of the platoon.

In the absence of the shielding effect, all bodies would have a drag ratio of 1 (by definition). However, the benefit of tandem operation is obvious for all combinations of the two simple shapes. The behavior of the drag ratios suggests the existence of two separate length scales: Over a separation $S/\sqrt{A}$ of the order of 1, the drag ratios start out much lower than one, then quickly rise to a local maximum at approximately $S/\sqrt{A}=1$. As the bodies are separated further, the drag levels actually drop before rising again but at a much steadier pace. Of course, each drag ratio is expected to reach one asymptotically, which would appear to take place over a longer length scale of approximately $S/\sqrt{A}=10$, though our measurement range is not large enough to cover this range.

The two length scales characterize two types of interaction; a strong one in the range $S/\sqrt{A}=0\text{-}1$ and a weak one in the range $S/\sqrt{A}=1\text{-}10$. In the strong interaction range of separation, the drag on the front body starts out at about 70%-90% of the isolation value depending on whether it is rounded or blunt, respectively. In contrast, the drag on the rear body starts out at a much lower level of only 20% of the isolation value (for blunt) and 40% (for rounded).
Both bodies experience lower drag as a result of the tandem configuration, with the rear body generally experiencing a higher drag reduction compared to the isolation values. However, the case of two rounded bodies bucks the trend; the rear body has lower relative drag in the strong interaction region, but the reverse is true in the weak interaction region.

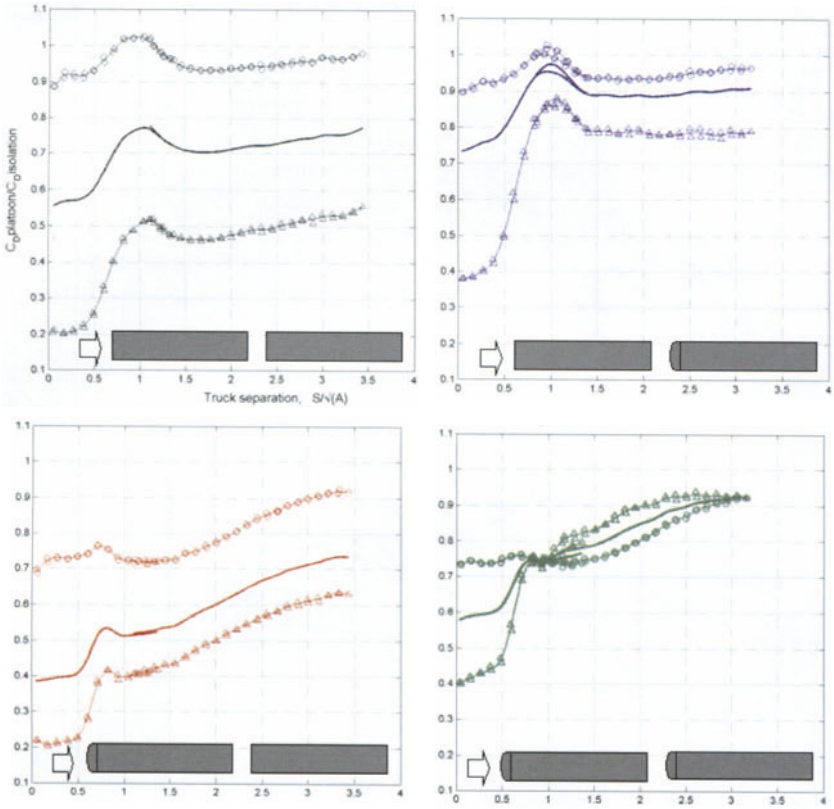

Figure 16. Drag curves for various combinations of simplified bodies. o front-body drag; Δ rear-body drag; ___ average drag. (a) blunt lead and trail; (b) blunt lead - rounded trail; (c) rounded lead- blunt trail; (d) rounded lead and trail.

The total drag savings for the pair of bodies is given by the plot of average drag ratio as defined earlier. The average drag ratios for the four configurations are plotted on Figure 17.

The tandem configuration that experiences the least amount of total drag is that of a rounded body in the front and a blunt body in the rear. Conversely, when the relative positions of the two bodies are switched, the highest possible total drag results. Note that when the two bodies are identical, the total drag ratio is essential identical in the region of strong interaction, regardless of whether the bodies are both rounded or both blunt. As the gap is increased beyond S/√A=1, the tandem of two blunt bodies experiences further drag ratio drop and starts to behave like the lowest drag case (rounded followed by blunt) as S/√A approaches 3.5. On the other hand, the tandem of two rounded bodies sees an increasing drag ratio with increasing gap spacing, and gradually converges to the highest drag case (blunt followed by rounded). As S/√A increases beyond 2.5, the pair of rounded bodies in tandem appears to benefit less and less from the tandem configuration; the

weakening interaction between bodies is a manifestation of the law of diminishing returns.

The reason for the superiority of the rounded-blunt combination to the blunt-blunt configuration is explained again by separating the drag into contributions from fore-body and base. Almost all of the differences between blunt-blunt and rounded-blunt come from savings for the lead body in the latter case, as Figure 16 will attest. The drag reduction is greater in the latter case because roughly half the total drag of rounded forward body is base drag that is greatly diminished by the presence of the trail body at short spacing. Conversely, most of the drag from blunt forward body comes from the fore-body, which is too far removed to be influenced much by the trail body.

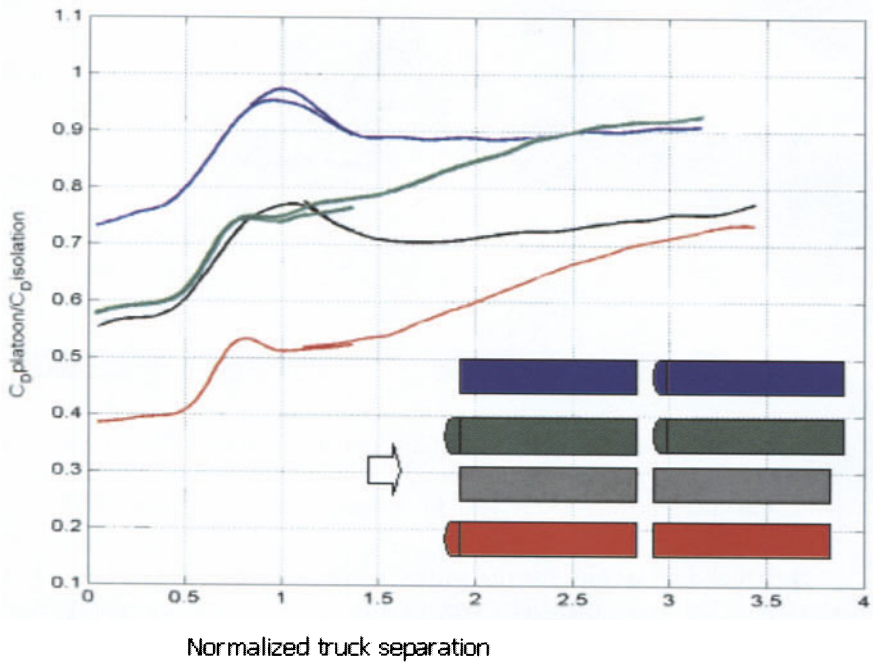

Figure 17. Summary of average drag of platoon for all four configurations.

Hence it is clear that drag savings depend upon the drags of individual trucks in isolation, and upon which truck is leading. For completeness, measurements are made with more realistic truck models, as shown in Figure 18. The trucks have wheels, and the drag of each truck is artificially increased by introducing drag-enhancing elements, such as the netting spoken of earlier, by providing a gap between the tractor and trailer, and by providing additional drag enhancing "collars". The drag collars consist of a series of short, protruding cylinders ringing the trailer at a particular station. They are meant to provide an increase in drag by increasing the boundary layer momentum thickness. Various combinations that either include or exclude netting collars,

or gap, result in truck models having drag coefficients in isolation in the range $C_D \approx 0.5 - 0.7$.

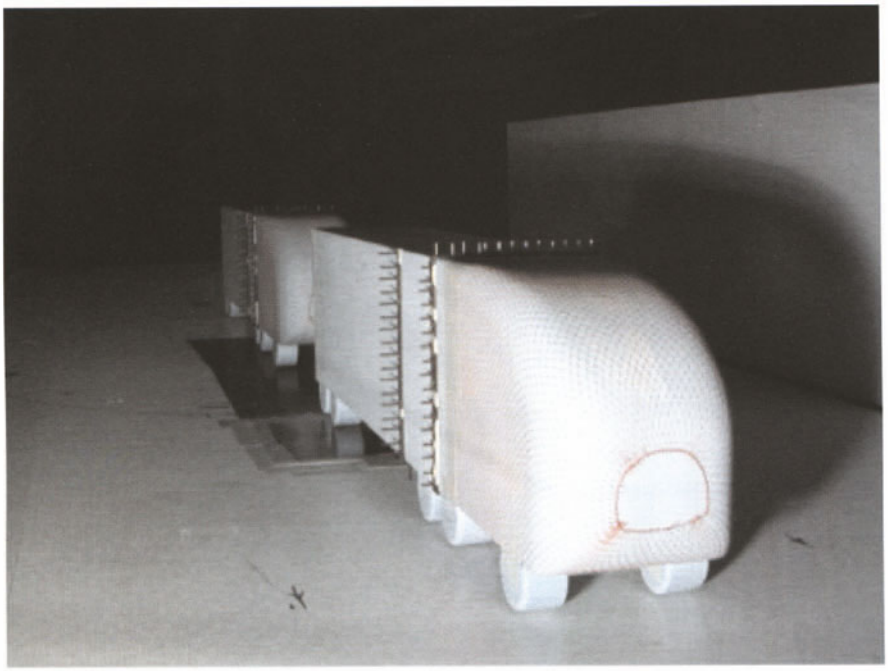

Figure 18. Truck models in tandem configuration. With netting and "collars", the C_D for each truck in isolation ≈ 0.7.

The drag data for the realistic models is plotted in Figure 19. The data points collapse on a single curve within the range covered by the simplified shapes. This indicates that the data total drag savings for the models in Figure 18 in tandem is independent of the choice of leading and trailing truck. Note also that the drag ratio rises gradually with gap spacing and that the local maxim at $S/\sqrt{A}=1$ vanishes. The effect of the critical gap is not so dramatic for models having a distributed drag including wheels and drag collars.

Also, the entire data set is bounded by the "blunt - rounded" and "rounded - blunt" cases on the upper and lower end, respectively. These limiting cases delineate the maximum and minimum drag savings for any tandem configuration. For comparison purposes, the road test data of Bonnet & Fritz (2000) (who used real trucks) is included, along with its computed average. The average drag ratio for the road test appears to agree best with the "blunt – blunt" and "rounded – blunt" where there is overlap.

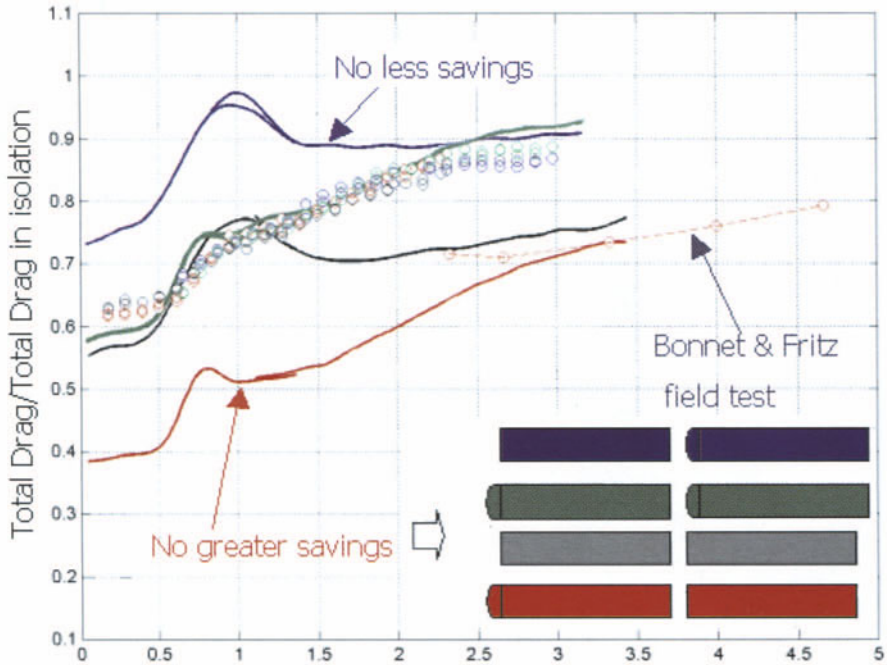

Figure 19. Average drag of platoons. The circles represent data obtained by arranging the models shown in Figure 18 in various tandem combinations.

Summary Conclusions

The present experiments reveal the impact of on the drag of a single tractor-trailer truck. A combination of force balance and whole-field velocity measurements demonstrates a direct link between the level of drag forces and the nature of the fluid flow patterns within the gap. At moderate widths a stable toroidal vortex is present in the gap and drag levels are relatively low. The symmetry of the flow pattern breaks down at a width of approximately half the square-root of frontal area, which leads to intermittent flow separation off the front of the trailer and a non-linear increase of drag forces on the trailer and on the truck as whole. Most of the drag contribution is attributed to the trailer alone; the tractor is affected much more moderately and only in a narrow band of gap width near the critical value of $G/\sqrt{A} \approx 0.5$. A similar process of drag rise also occurs at moderate angles of yaw. However, the drag increase is more pronounced and occurs at a lower critical gap width as the angle of yaw is increased. At more extreme angles of yaw the tractor and trailer are rather like independent bodies that do not benefit from close-formation and their drag behavior is much less a function of spacing.

The benefits of close-formation also apply to trucks in tandem. The total drag for all tandems tested is lower than the sum of the drags of the models in isolation, though the drag savings vary with the degree of bluntness of each

model and on which model is placed in front. The highest relative drag reduction is achieved by a rounded model followed by a blunt model, while the reverse order achieves the least drag reduction.

References

K. R. Cooper: The effect of front-edge rounding and rear-edge shaping on the aerodynamic drag of bluff vehicles in ground proximity. SAE paper No. 850288 (1985)

A.M. Fincham & G.R. Spedding: Low cost, high resolution DPIV for measurement of turbulent fluid flow. Exps. Fluids **23**, (1997)

C. Bonnet & H. Fritz: Fuel consumption reduction experienced by two Promote-Chauffeur trucks in electronic tow bar operation. SAE Paper No. 00FTT73 (2000).